Syntheses, Crystal Structures and Inhibitory Activity against MCF-7, NCI-H460 and HepG2 Cancer Cells of the Di-2,4-dichlorobenzyltin Thiophene-2-carbohydrazone Complexes①

XU Jia-Chi[a] HU Ze-Cheng[a] CUI Ying[b]
JIANG Wu-Jiu[b] TAN Yu-Xing[b] FAN Shan-Ji[a]②

[a] (*Department of Thyroid Breast Surgery, The First Affiliated Hospital of University South China, Hengyang* 421001, *China*)

[b] (*Hengyang Normal University, Hengyang* 421008, *China*)

ABSTRACT Di-2,4-dichlorobenzyltin-2-(2-(thiophen-2-formyl)hydrazono)-propanoic carboxylate complex **I** $\{[C_4H_3S(O)C=N-N=C(CH_3)COO]_2[(2,4\text{-}Cl_2\text{-}C_6H_3CH_2)_2Sn](CH_3OH)_2\}$ and di-2,4-dichlorobenzyltin-2-(2-(thiophen-2-formyl)hydrazono)-3-phenylpropanoic carboxylate complex **II** $\{[C_4H_3S(O)C=N-N=C(PhCH_2)COO](2,4\text{-}Cl_2\text{-}C_6H_3CH_2)_2Sn\}_n$ were synthesized and characterized by IR, ^{1}H, ^{13}C and ^{119}Sn NMR spectra, HRMS, elemental analysis and thermal stability analysis, and the crystal structures were determined by X-ray diffraction. The crystal of complex **I** belongs to monoclinic system, space group $P2_1/n$ with a = 11.987(3), b = 35.359(9), c = 12.982(3) Å, β = 103.028(5)°, Z = 4, V = 5361(2) Å^3, D_c = 1. 688 Mg ㎜$^{-3}$, μ(Mo$K\alpha$) = 1.463 mm^{-1}, F(000) = 2704, R = 0.0572 and wR = 0.1423. The crystal of complex **II** is of monoclinic system, space group $P2_1/n$ with a = 15.5758(17), b = 9.6020(10), c = 19.599(2) Å, β = 98.886(2)°, Z = 4, V = 2896.0(5) Å^3, D_c = 1.663 Mg ㎜$^{-3}$, μ(Mo$K\alpha$) = 1.357 mm^{-1}, F(000) = 1440, R = 0.0341 and wR = 0.0936. *In vitro* antitumor activities of both complexes were evaluated by MTT against three human cancer cell lines (MCF7, NCI-H460 and HepG2), and they all exhibited good antitumor activity. The interaction between complexes and calf thymus DNA was studied by UV-vis and fluorescence spectroscopy, it indicated intercalation as probable mode of interaction.

Keywords: diorganotin, carboxylate, synthesis, crystal structure, biological activity;
DOI: 10.14102/j.cnki.0254–5861.2011–3007

1 INTRODUCTION

Currently, the incidence of cancer is increasing year by year, and the metastasis and drug resistance of cancer are still the most difficult problems in the clinical treatment. Platinum drugs are the most widely used metal drugs in the clinical treatment of cancer[1], such as cisplatin, carboplatin, and oxaliplatin. However, due to the long-term use of platinum drugs, its defects have also emerged. The efficacy of platinum drugs has been severely restricted by toxic side effects and acquired drug resistance[2-7]. Therefore, the design and development of new metal antitumor complexes have great theoretical and practical significance.

Organotin compounds have the advantages of good biological activity and easy modification of the structure[8]. The anti-tumor activity of the complex can be adjusted by fine-tuning the structure. Therefore, the introduction of ligand molecules with different physiological functions into the complex will help regulate the biological activity of the organotin complex, expand the chemical space as much as possible, and maximize the function of the complex. Based on our previous work[9-11], two unreported organotin complexes were prepared by the furan heterocyclic ligand with bis(2,4-dichlorobenzyl)tin dichloride, and their effects on cancer cells and the mechanism of interaction with calf thymus DNA were studied preliminarily, which provides an

Received 25 October 2020; accepted 7 January 2021 (**CCDC 2039992 and 2039993**)

① Supported by the Natural Science Foundation of Hunan Province (No. 2020JJ8096)

② Corresponding author. E-mail: firear333@hotmail.com

Xu Jia-Chi and Hu Ze-Cheng made equal contributions to this work

important theoretical basis for making up the shortage of clinical platinum drugs as well as for the treatment of tumor diseases and the development of new metal antitumor drugs.

2 EXPERIMENTAL

2. 1 Instruments and reagents

Infrared spectrum (KBr) was recorded by the Prestige-21 infrared spectrometer (Japan Shimadzu, 4000～400 cm^{-1}). ^{1}H, ^{13}C and ^{119}Sn NMR spectra were measured with a Bruker AVANCE-500 NMR spectrometer. The elemental analysis was determined by PE-2400(II) elemental analyzer. Crystallographic data of the complexes were collected on a Bruker SMART APEX II CCD diffractometer. HRMS was measured with the Thermo Scientific LTQ Orbitrap XL (ESI source). Melting points were determined using an X4 digital microscopic melting point apparatus without correction (Beijing Tektronix Instrument Co. Ltd.). Thermogravimetric analyses (TGA) were recorded on a NETZSCH TG 209 F3 instrument at a heating rate of 20 ℃·min^{-1} from 40 to 800 ℃ under air. The UV spectra were determined with the UV-2550 spectrophotometer (Shimazu). Fluorescence spectra were obtained with a Hitachi F-7000 spectrophotometer with quartz cuvette (path length = 1 cm).

2-(2-(Thiophen-2-formyl)hydrazono)-propanoic acid, 2-(2-(thiophen-2-formyl)hydrazono)-3-phenylpropanoic acid ligand and di-2,4-dichlorobenzyltin dichloride were prepared according to the literatures[12]. Ethidium bromide (EB), calf thymus DNA and three hydroxymethyl aminomethanes (tris) were from Sigma-Aldrich LLC. Carboplatin was from J&K Scientific Ltd. Dibutyltin oxide was from Alfa Aesar (China) Chemical Co., Ltd. Other chemicals were from Sinopharm Chemical Reagent Co., Ltd. All reagents were of analytical grade obtained from commercial sources and used without further purification. The human breast cancer cells (MCF-7, ATCC No: HTB-22), human lung cancer cells (NCI-H460, ATCC No: HTB-177) and human liver cancer cells (HepG2, ATCC No: HB-8065) were obtained from American Tissue Culture Collection (ATCC). Culture media RPMI-1640 (10.0%) were purchased from USA GIBICO. Ultrapure water (18.2 MΩ·cm) obtained from a Milli-Q water purification system (Millipore Co., USA) was used in all experiments. Tris-HCl (0.01 mol L^{-1}) buffer solution was prepared by a certain amount of tris dissolved in super-pure water before using, and the pH of the solution was adjusted to 7.40 with hydrochloric acid solution (0.1 mol L^{-1}). The purity of CT-DNA was determined by comparing the absorbance at 260 and 280 nm (A_{260}/A_{280} = 1.8～1.9/1). The concentration of CT-DNA was calculated by measuring the absorbance at 260 nm (ε_{260} = 6600 L·mol^{-1}·cm^{-1}). The reserve solution was stored at 4 ℃. The ethidium bromide solution was prepared by a certain amount of ethidium bromide solid dissolved in tris-HCl (0.01 mol L^{-1}) buffer solution.

2. 2 Synthesis of the complexes

A mixture of 2-(2-(thiophen-2-formyl)hydrazono)-propanoic acid (1.0 mmol), di-2,4-dichlorobenzyltin dichloride (1.0 mmol) and CH_3OH (20.0 mL) was added in a round-bottomed flask (50.0 mL), and refluxed with stirring for 6.0 h. Then the mixture was cooled and filtered. The complex crystals were obtained by controlling solvent evaporation. Complex **I** was red crystal. Yield: 70%. m.p.: 181～183 ℃. Anal. Calcd. ($C_{46}H_{40}Cl_8N_4O_8S_2Sn_2$): C, 40.56; H, 2.96; N 4.11%. Found: C, 40.77; H, 3.01; N, 4.19%. UV-vis (DMSO+H_2O) λ_{max}: 358 nm. FT-IR (KBr, cm^{-1}): 3458 ν(-OH), 3098 ν(=C–H), 2934, 2828 ν(-C–H), 1593, 1385 ν(COO), 1612 ν(C=N), 656 ν(Sn–O), 590 ν(Sn–O–Sn), 511 ν(Sn–N), 446 ν(Sn–C). ^{1}H NMR (500 MHz, $CDCl_3$, δ/ppm): 7.56 (dd, J_1 = 3.7 Hz, J_2 = 1.2 Hz, 2H), 7.53 (dd, J_1 = 5.0 Hz, J_2 = 1.2 Hz, 2H), 7.20 (d, J = 2.1 Hz, 4H), 7.08 (s, 1H), 7.07 (d, J = 1.2 Hz, 1H), 7.06 (d, J = 8.1 Hz, 4H), 6.95 (dd, J_1 = 8.1 Hz, J_2 = 2.2 Hz, 4H), 3.50 (s, 6H), 3.29 (d, J = 12.1 Hz, 4H), 3.18 (d, J = 12.1 Hz, 4H), 2.44 (s, 6H). ^{13}C NMR (126 MHz, $CDCl_3$, δ/ppm): 170.68, 164.67, 153.67, 136.19, 133.36, 133.15, 132.15, 132.05, 131.64, 131.24, 128.77, 127.72, 127.17, 50.84, 30.00, 13.67. ^{119}Sn NMR (187 MHz, $CDCl_3$, δ/ppm): –292.11. HRMS (ESI) m/z calcd. for $C_{22}H_{17}Cl_4N_2O_3SSn^+$ $[M–CH_3OH+H]^+$ 648.8731, found 648.8698.

Complex **II** was prepared in a similar procedure (Fig. 1) as **I** by 2-(2-(thiophen-2-formyl)hydrazono)-propanoic acid (1.0 mmol) in place of 2-(2-(thiophen-2-formyl)hydrazono)-3-phenylpropanoic acid. The product was yellow crystal with the yield of 80%. m.p.: 242～245 ℃. Anal. Calcd. ($C_{28}H_{20}Cl_4N_2O_3SSn$): C, 46.38; H, 2.78; N, 3.86%. Found: C, 46.44; H, 2.98; N, 3.82%. UV-vis (DMSO+H_2O) λ_{max}: 340 nm. FT-IR (KBr, cm^{-1}): 3057, 3030 ν(=C–H), 2934, 2843 ν(C–H), 1593, 1417 ν(COO), 1645 ν(C=N), 656 ν(Sn–O), 588 ν(Sn–O–Sn), 507 ν(Sn–N), 444 ν(Sn–C). ^{1}H NMR (500 MHz, $CDCl_3$, δ/ppm): 7.63 (dd, J_1 = 3.8 Hz, J_2 = 1.2 Hz, 1H), 7.58 (dd, J_1 = 5.0 Hz, J_2 = 1.2 Hz, 1H), 7.47 (d, J = 7.5 Hz, 2H), 7.29～7.32 (m, 2H), 7.12 (dd, J_1 = 5.0 Hz, J_2 = 3.8 Hz, 1H), 7.04 (d, J = 1.4 Hz, 2H), 6.90 (d, J = 8.4 Hz, 2H), 6.80

(dd, J_1 = 8.4 Hz, J_2 = 1.4 Hz, 2H), 4.19 (s, 2H), 3.19 (d, J = 12.2 Hz, 2H), 3.09 (d, J = 12.2 Hz, 2H). ^{13}C NMR (126 MHz, $CDCl_3$, δ/ppm): 170.74, 136.29, 134.39, 133.35, 132.84, 132.40, 132.07, 131.87, 130.95, 130.27, 129.78, 128.77, 128.66, 127.84, 127.13, 32.69, 29.39. ^{119}Sn NMR (187 MHz, $CDCl_3$, δ/ppm): –275.18. HRMS (ESI) m/z calcd. for $C_{28}H_{21}Cl_4N_2O_3SSn^+$ $[M+H]^+$ 724.9043, found 724.9025.

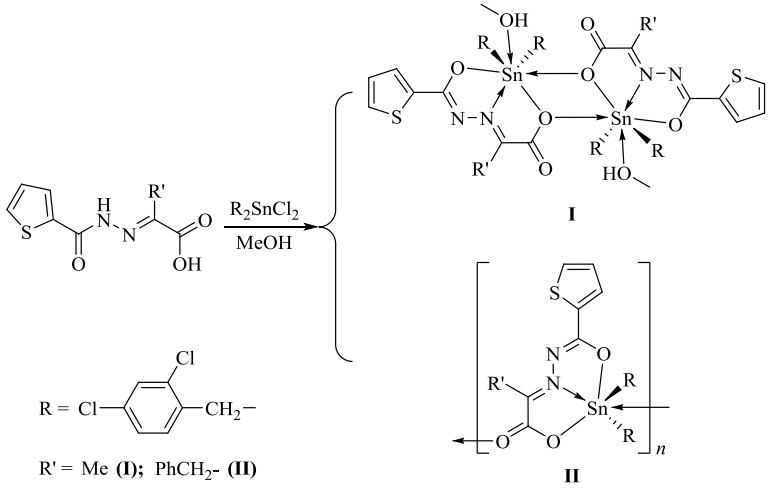

Fig. 1. Syntheses of the complexes

2. 3 Crystal structure determination

Suitable single crystals with dimensions of 0.21mm × 0.20mm × 0.20mm (**I**) and 0.22mm × 0.21mm × 0.21mm (**II**) were selected for data collection at 296(2) K on a Bruker SMART APEX II CCD diffractometer equipped with graphite-monochromated Mo$K\alpha$ radiation (λ = 0.071073 nm) using a φ-ω mode. All the data were corrected by Lp factors and empirical absorbance. The structure was solved by direct methods. All non-hydrogen atoms were determined in successive difference Fourier synthesis, and hydrogen atoms were added according to theoretical models or located from the Fourier maps. All hydrogen and non-hydrogen atoms were refined by their isotropic and anisotropic thermal parameters through full-matrix least-squares techniques. All calculations were completed by the SHELXTL-97[13] program. For complex **I**, a total of 27192 reflections were obtained in the range of 1.71<θ<25.10 ° with 9539 unique ones (R_{int} = 0.0575), S = 1.050, $(\Delta\rho)_{max}$ = 1.348 and $(\Delta\rho)_{min}$ = –0.712 e/Å^3, max transmission was 0.7586, min transmission was 0.7487, and the completeness was 99.8%. For complex **II**, a total of 14281 reflections were obtained in the range of 1.81<θ<25.10 ° with 5144 unique ones (R_{int} = 0.0190), S = 1.039, $(\Delta\rho)_{max}$ = 1.207, $(\Delta\rho)_{min}$ = –0.658 e/Å^3, max transmission was 0.7637, min transmission was 0.7545, and the completeness was 99.8%. The selected bond lengths and bond angles for **I** and **II** are listed in Table 1.

Table 1. Selected Bond Lengths (Å) and Bond Angles (°) for I and II

I					
Bond	Dist.	Bond	Dist.	Bond	Dist.
Sn(1)–C(9)	2.22(3)	Sn(2)–C(32)	2.150(7)	Sn(1)–O(1)	2.161(4)
Sn(1)–C(16)	2.144(6)	Sn(2)–C(39)	2.144(7)	Sn(1)–O(2)	2.339(4)
Sn(1)–O(4)	2.412(5)	Sn(1)–N(1)	2.230(5)	Sn(2)–O(5)	2.146(4)
Sn(2)–O(6)	2.335(4)	Sn(2)–O(8)	2.437(5)	Sn(2)–N(3)	2.233(5)
Angle	(°)	Angle	(°)	Angle	(°)
C(16)–Sn(1)–O(1)	95.5(2)	C(16)–Sn(1)–O(4)	84.2(2)	C(32)–Sn(2)–N(3)	96.2(2)
C(16)–Sn(1)–C(9)	162.2(11)	O(1)–Sn(1)–O(4)	76.64(18)	C(39)–Sn(2)–O(6)	87.9(2)
O(1)–Sn(1)–C(9)	96.7(9)	C(9)–Sn(1)–O(4)	86.1(11)	O(5)–Sn(2)–O(6)	140.85(15)
C(16)–Sn(1)–N(1)	96.6(2)	N(1)–Sn(1)–O(4)	147.82(19)	C(32)–Sn(2)–O(6)	90.2(2)
O(1)–Sn(1)–N(1)	71.25(19)	O(2)–Sn(1)–O(4)	142.14(17)	N(3)–Sn(2)–O(6)	69.83(17)
C(9)–Sn(1)–N(1)	99.5(12)	C(39)–Sn(2)–O(5)	96.4(2)	C(39)–Sn(2)–O(8)	86.5(2)
C(16)–Sn(1)–O(2)	91.4(2)	C(39)–Sn(2)–C(32)	160.2(3)	O(5)–Sn(2)–O(8)	75.41(18)

To be continued

O(1)–Sn(1)–O(2)	141.19(17)	O(5)–Sn(2)–C(32)	97.5(2)	C(32)–Sn(2)–O(8)	83.5(2)
C(9)–Sn(1)–O(2)	87.1(9)	C(39)–Sn(2)–N(3)	101.6(2)	N(3)–Sn(2)–O(8)	146.27(19)
N(1)–Sn(1)–O(2)	70.03(17)	O(5)–Sn(2)–N(3)	71.20(17)	O(6)–Sn(2)–O(8)	143.73(17)
II					
Bond	Dist.	Bond	Dist.	Bond	Dist.
Sn(1)–C(22)	2.128(4)	Sn(1)–O(2)	2.158(2)	Sn(1)–O(1)	2.226(2)
Sn(1)–C(15)	2.138(4)	Sn(1)–N(1)	2.199(3)	Sn(1)–O(3)^{i}	2.515(2)
Angle	(°)	Angle	(°)	Angle	(°)
C(22)–Sn(1)–C(15)	145.54(16)	O(2)–Sn(1)–N(1)	73.23(9)	C(22)–Sn(1)–O(3)^{i}	78.94(12)
C(22)–Sn(1)–O(2)	100.13(14)	C(22)–Sn(1)–O(1)	90.90(13)	C(15)–Sn(1)–O(3)^{i}	80.66(13)
C(15)–Sn(1)–O(2)	100.91(12)	C(15)–Sn(1)–O(1)	88.34(13)	O(2)–Sn(1)–O(3)^{i}	74.75(9)
C(22)–Sn(1)–N(1)	103.27(13)	O(2)–Sn(1)–O(1)	143.22(9)	N(1)–Sn(1)–O(3)^{i}	147.79(9)
C(15)–Sn(1)–N(1)	108.78(13)	N(1)–Sn(1)–O(1)	70.09(9)	O(1)–Sn(1)–O(3)^{i}	142.02(9)

Symmetry codes (II) ^{i} $-x+3/2, y-1/2, -z+3/2$

2. 4 *In vitro* anti-tumor activity assays

The synthesized compounds were dissolved in DMSO at a concentration of 50 mM as stock solution. To avoid DMSO toxicity, the concentration of DMSO was less than 0.1% (v/v) in all experiments. MCF7, NCI-H460 and HepG2 cells were cultured in RPMI-1640 medium supplemented with 10% fetal bovine serum (FBS) and grown at 37 ℃ in a saturated humidified atmosphere in the presence of 5.0% (volume fraction) CO_2. Cell proliferation was assessed by MTT assay. 100 μL of cells (5×10^7 cells·L^{-1}) incubated at 37 ℃, 5% CO_2 was seeded into 96 well plates. Then the medium was replaced with the respective medium containing complexes at different concentrations and incubated for 48 h. 10 μL of MTT was added and the medium was removed after 4 h of incubation. Finally, crystal violet was solubilized in 100 μL DMSO and the absorbance was measured at 570 nm. Six concentrations (0.5～50 μM) were set for the compounds and at least 3 parallels of every concentration were used. All experiments were repeated at least three times. The data were calculated using Graph Pad Prism version 7.0. The IC_{50} was fitted using a non-linear regression model with a sigmoidal dose response.

2. 5 Interaction with DNA

The investigation of the possible binding modes of complex to DNA and the calculation of the corresponding DNA-binding constants (K_b) were carried out by UV-vis spectroscopy. UV-visible absorption spectrometry experiments were carried out with a constant concentration of I (50 μM) varying the concentration of CT-DNA (0～80 μM) in tris-HCl (0.01 mol·L^{-1}) buffer solution. The intrinsic binding constant (K_b) was calculated according to the following Wolfe-Shimmer equation[14]:

$$c_{DNA}/(\varepsilon_A - \varepsilon_F) = c_{DNA}/(\varepsilon_B - \varepsilon_F) + 1/K_b(\varepsilon_B - \varepsilon_F)$$

Where c_{DNA} is the concentration of CT-DNA, ε_A the observed extinction coefficient at arbitrary DNA concentration, ε_F the extinction coefficient of the free complex, and ε_B the extinction coefficient of the complex when fully combined to CT-DNA. The DNA-binding constant K_b, the ratio of the slope to intercept, was determined by the Wolfe-Shimmer equation and the plot $c_{DNA}/(\varepsilon_A - \varepsilon_F)$ versus c_{DNA}.

In the fluorescence study, a mixture of CT-DNA (30 μM), EB (3 μM) and different concentration complex **I** solution (0～80 μM) was placed in a 5 mL volumetric flask in tris-HCl (0.01 mol·L^{-1}) buffer solution[15, 16]. After 3 h, the fluorescence spectra were acquired at 25 ℃. The excitation wavelength was 258 nm, and the emission wavelength is shown in the spectrum. The slit scanning width of emission and excitation is 5.0 nm. Finally, the quenching constant (K_{sv}) values of **I** were determined by using the Stern-Volmer equation[17].

3 RESULTS AND DISCUSSION

3. 1 Spectral analyses

The FT-IR spectra of complexes **I** exhibit characteristic absorption of hydroxyl group appearing at 3458 cm^{-1}, which can be ascribed to the presence of coordinated methanol molecules. In **I** and **II**, the asymmetric and symmetric stretching vibrations of carbonyl group are as follows: ν_{as}(COO) = 1593 and ν_s(COO) = 1385 cm^{-1} (**I**), ν_{as}(COO) = 1593 and ν_s(COO) = 1417 cm^{-1} (**II**), $\Delta\nu$ = 208 (**I**), 176 cm^{-1} (**II**), suggesting that the carboxyl groups of complex **I** are coordinated with Sn atoms in a monodentate manner, while those of **II** are bridging coordination[18]. In **I**, the characteristic peaks of ν(Sn–O), ν(Sn–O–Sn), ν(Sn–N) and ν(Sn–C) occur at 656, 590, 511 and 446 cm^{-1}, and the same characteristic peaks of **II** are located at 656, 588, 507 and 444

cm^{-1}[19], respectively, which indicate similar structures for both complexes. The above results are confirmed by single-crystal X-ray diffraction analysis.

In the ^{1}H NMR spectrum, the integral area ratio of each peak is consistent with the number of protons in each group of the expected structure[20]. The hydrogen proton absorption peaks of the aryl ring of complexes **I** and **II** are observed at 6.95～7.56 and 6.80～7.63 ppm in the low field, respectively. The benzylic methylene protons in ligand appear at 3.18～3.29 (**I**) and 3.08～3.19 (**II**) ppm. The benzylic methylene protons connected with Sn in complexes present two double peaks. It is speculated that complexes cannot be freely rotated due to their large steric hindrance, resulting in the geminal coupling[10].

The ^{13}C NMR spectra show carbon atoms from carboxyls of **I** and **II** have the same peak positions, and the peaks of other groups are consistent with the number of structural carbon atoms theoretically speculated[18]. It can be inferred from the positions of hydrogen proton and carbon peaks of both complexes that **I** and **II** have similar structures, which is consistent with the results of X-ray single-crystal diffraction.

The ^{119}Sn NMR spectrum indicates Sn-core peaks of **I** and **II** are a single peak with –292.11 and –275.18 ppm, respectively, showing the existence of a single organotin complex in both complexes.

In HRMS spectra, mass spectral peaks of complex **I** appear at *m*/*z* 648.8698, which can be attributed to the absorption peaks of [M-CH_3OH+H]$^+$. Complex **II** is found at *m*/*z* 724.9025 due to the absorption peaks of [M+H]$^+$.

3. 2 Structure description

As shown in Fig. 2, complex **I** is a noncentrosymmetric dimer distannoxane. There is a Sn_2O_2 four-membered ring in the middle of the molecule. In the four-membered Sn_2O_2 ring, the sum of the interior angles is 360 °, indicating the four-membered Sn_2O_2 ring is planar. But the bond lengths of two Sn–O are not equal: Sn(1)–O(2) 2.339, Sn(1)–O(6) 2.721, Sn(2)–O(2) 2.717 and Sn(2)–O(6) 2.333 Å. Sn(1) is seven-coordinated by two oxygen atoms (O(1) and O(2)) from the ligand, one imino nitrogen atom (N(1)), one oxygen atom (O(4)) from the coordination alcohol, two methylene carbon atoms (C(9) and C(16)) from two di-2,4-dichlorobenzyl groups, and O(6) from another ligand molecule. Atoms O(1), O(2), O(5), N(1) and O(6) occupy the equatorial plane, while C(9) and C(16) locate at the axial positions to form a seven-coordinated pentagonal bipyramidal configuration. The axial angle C(9)–Sn(1)–C(16) is 162.24 °, which deviates from 17.76 ° by 180 °. In addition, the bond lengths and bond angles around Sn(1) are different, so the geometry around Sn(1) can be best described as a distorted pentagonal bipyramidal configuration, so Sn(2) is similar to Sn(1).

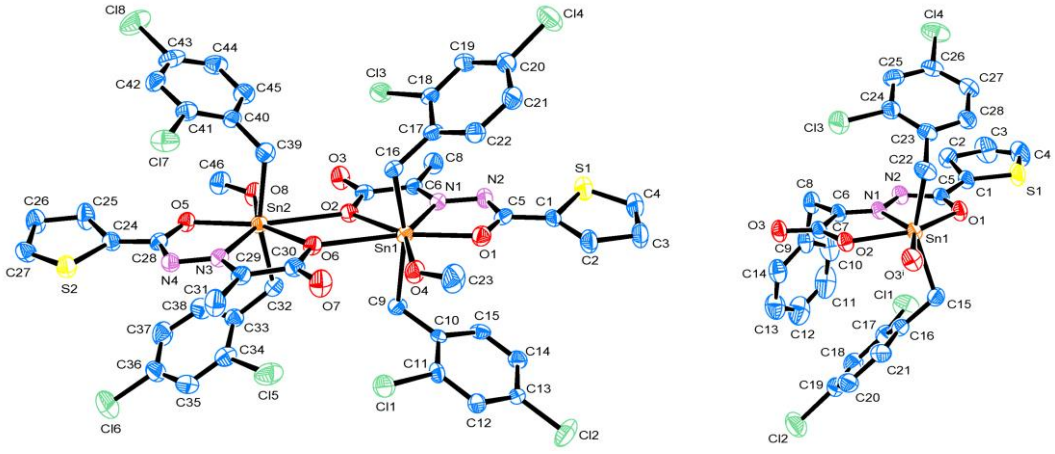

Fig. 2. Molecular structures of I (a) and II (b). Symmetry code for II: ^{i} –*x*+3/2, *y*–1/2, –*z*+3/2

In complex **II**, the central tin atoms are all six-coordinated in a distorted octahedral configuration. The bond length of Sn(1)–O(3)^i is 2.514 Å, which belongs to normal Sn–O covalent bond length, proving a strong interaction between Sn(1) and O(3)^i. Therefore, the one-dimensional infinite chain structure is formed by Sn(1)–O(3)^i (Fig. 3).

In both complexes, the bond lengths of Sn–N are 2.229, 2.234 Å (**I**) and 2.199 Å (**II**), similar to those observed in literature[21].

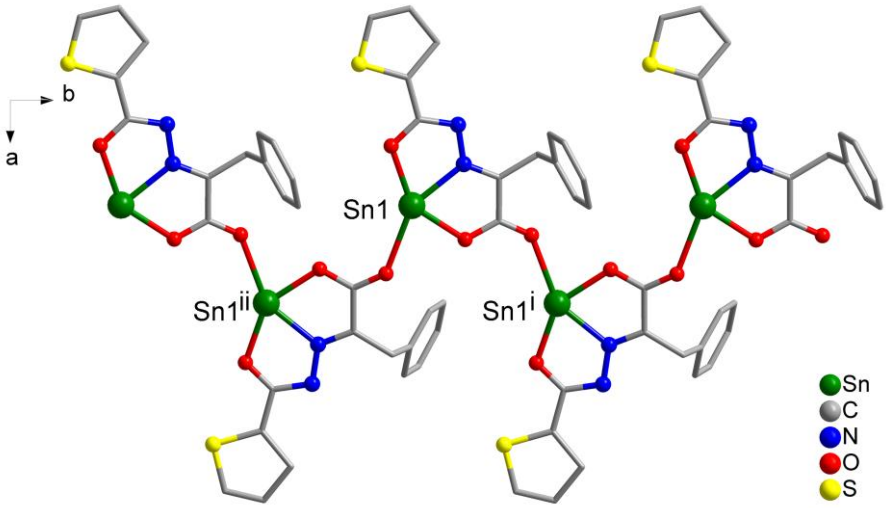

Fig. 3. 1*D* infinite chain structure of II. The 2,4-dichlorobenzyl group on the tin atom is omitted for clarity

3. 3 Thermal stability

Thermal stabilities of both complexes are carried out using a NETZSCH TG 209 F3 thermogravimetric analyzer from 40 to 800 ℃ at a rate of 20 ℃ min^{-1} under an air atmosphere at a flowing rate of 20.0 mL min^{-1}. As shown in Fig. 4, complex **I** displays a small weight loss at around 150 ℃, corresponding to the loss of methanol molecule, but this weight loss does not appear in the thermogravimetric curve of **II**. Thereafter, it explains that there is methanol involved in coordination in **I**, and the results were consistent with X-ray single-crystal diffraction data. In the next stages, both complexes suffer complete decomposition until 800 ℃, corresponding to the removal of ligand and the 2,4-dichlorobenzyl group attached to the tin atom. The remaining weight (22.48% (**I**) and 19.44% (**II**)) indicates the final products are SnO_2 (22.13% (**I**) and 20.79% (**II**)). In summary, **I** and **II** are rather stable up to about 240 and 220 ℃, respectively.

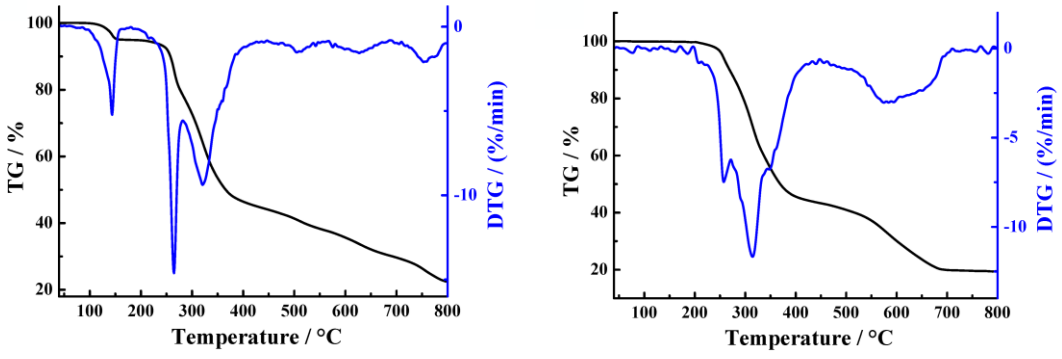

Fig. 4. TG-DTG curves for I (a) and II (b)

3. 4 Anticancer activity

The *in vitro* antitumor activities of all these ligands and complexes were evaluated by MTT assay against MCF-7, NCI-H460 and HepG2 cell lines, using carboplatin as the positive control. The tested results are shown in Table 2, where except for the IC_{50} of ligand **I** to HepG2 which is 37.61 ± 1.85 μM, the IC_{50} values of ligand **I** or **II** to other cancer cells are both greater than 50 μM. Complexes **I** and **II** have obvious inhibitory effects on these three cancer cells and they are better than carboplatin and ligands. Among three cancer cells, complex **I** is also the most sensitive to MCF-7 with IC_{50} of 4.11 ± 0.07 μM. In NCI-H460 and HepG2 cancer cells, complexes **I** and **II** have similar inhibitory activity. It can be found that the molecular structure difference between **I** and **II** is only the alkyl group attached to ligand by crystal structure analysis. Based on this observation, the possible structure-activity relationship can be recognized as follows. The anti-cancer activity of the ligand is generally worse than

that of the complex, and its anti-cancer activity is significantly increased after the complex is formed. The substituent on the ligand has a slight effect on the anticancer activity, and the alkyl tin has a greater inhibitory effect. It is speculated that the substituent on the ligand may not be an effective pharmacophore; on the other hand, the di-2,4-dichlorobenzyltin complex has anticancer activity. It may be related to the synergistic effect of ligand and organotin. Therefore, **I** or **II** are expected to be further chemically optimized as a candidate complex for anticancer drugs.

Table 2. Inhibition Action of the Complexes to Cancer Cell *in vitro*

	IC_{50}/μM		
	MCF-7	NCI-H460	HepG2
Ligand **I**	＞50	＞50	37.61 ±1.85
Ligand **II**	＞50	＞50	＞50
Complex **I**	4.11 ±0.07	6.74 ±0.32	6.89 ±0.32
Complex **II**	5.02 ±0.11	6.56 ±0.19	6.02 ±0.35
Carboplatin	8.22 ±0.41	7.26 ±0.32	7.70 ±0.25

3. 5 Interaction with DNA

The UV-vis spectra of **I** or **II** in the absence and presence of CT-DNA are shown in Fig. 4. It can be seen from Fig. 5 that the decrease in absorbance occurs with the increase of DNA concentration. In other words, with the addition of increasing concentrations of DNA, the absorption bands exhibit hypochromism. The hypochromism is attributed to the intercalation of these complex into the DNA base pairs. From the absorption spectroscopy tests, K_b values of **I** or **II** are calculated to be 0.2 × 10^3 L mol^{-1} (r^2 = 0.987) and 0.25 × 10^3 L mol^{-1} (r^2 = 0.988), which is smaller to the reported complexes in literatures[22] and explains the intercalation of **I** or **II** and DNA is relatively weaker. It preliminarily indicates an intercalation in the interaction between **I** or **II** and DNA.

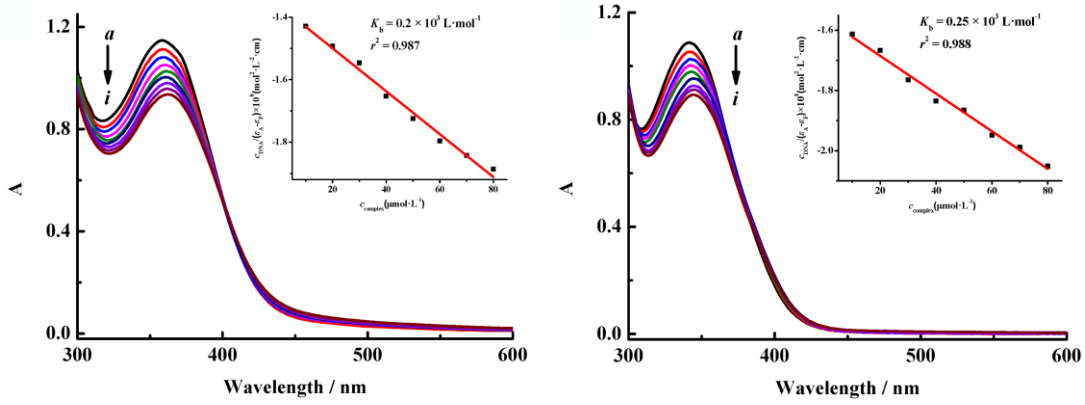

(a) **(b)**

Fig. 5. Electronic spectra of I (a) or II (b) in tris-HCl buffer upon addition of CT–DNA, $c_{complex}$ = 50 μmol L^{-1}; from *a* to *i*, c_{DNA} = 0, 10, 20, 30, 40, 50, 60, 70 and 80 μmol L^{-1}, respectively. The arrow shows the absorbance changes upon increasing DNA concentrations. Inset: plot of $c_{DNA}/(\varepsilon_A - \varepsilon_F)$ *vs.* $c_{complex}$

Fig. 6 shows the effects of **I** or **II** on the fluorescent spectra of EB-DNA system with different concentrations. With increasing the concentration, the fluorescence of EB-DNA complex system is quenched. Therefore, it is speculated the complexes can coordinate with the base groups of DNA molecule, resulting in that EB is squeezed out of the base pairs of the DNA molecule. To study quantificationally the binding capacity of complexes and DNA, we employed the classical Stern-Volmer equation[20] $I_0/I = 1 + K_{SV}c_{complex}$ to obtain the quenching constants K_{SV} of complexes replacing EB and DNA with 5.58 × 10^4 L mol^{-1} (**I**) and 4.66 × 10^4 L mol^{-1} (**II**). This value suggests the complexes insert in DNA to a certain degree. Furthermore, the quenching constants of **I** or **II** are comparable to those of similar reports in literatures[23]. As a result, we can describe the quenching principle as follows: the central Sn atom of complex is

combined with the base groups of DNA molecule, and the alkyl-substituted on tin is inserted into the DNA base pairs, and then they compete for EB to combine with DNA, thus resulting in EB to be squeezed out from the base pairs of DNA molecules.

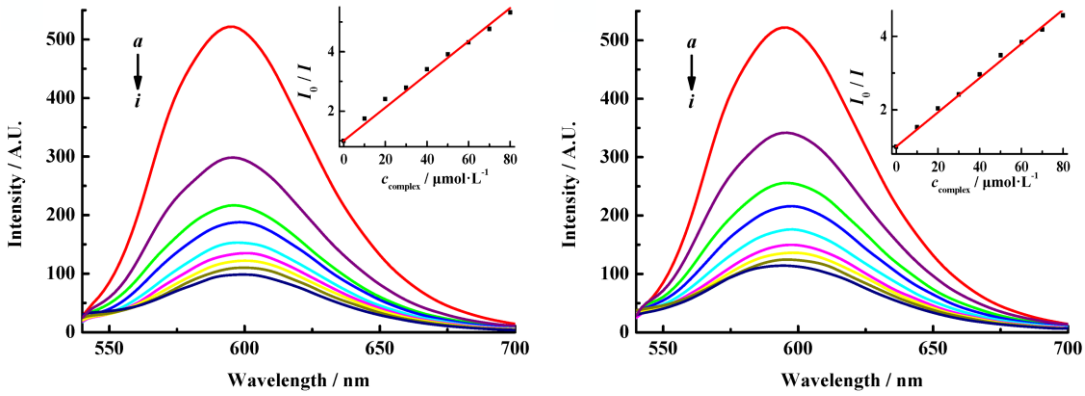

Fig. 6. Effects of I (a) or II (b) on the fluorescent spectra of EB-DNA system c_{CT-DNA} = 30 μmol·L^{-1}; c_{EB} = 3 μmol·L^{-1}; from *a* to *i*, $c_{complex}$ = 0, 10, 20, 30, 40, 50, 60, 70 and 80 μmol·L^{-1}, respectively; inset: plot of I_0/I *vs.* $c_{complex}$; λ_{ex} = 258 nm

4 CONCLUSION

Di-2,4-dichlorobenzyltin thiophene-2-carbohydrazone complexes were synthesized. Complex **I** shows a distorted seven-coordination pentagonal bipyramidal configuration and complex **II** is six-coordinated to form a distorted octahedral configuration. Complexes **I** and **II** are stable below 240 and 220 ℃, respectively. The inhibitory activities of **I** and **II** *in vitro* on cancer cells MCF-7, NCI-H460 and HepG2 were studied. **I** and **II** have obvious inhibitory effects on these three cancer cells. In *tris*-HCl buffer solution, the interaction between complexes **I** or **II** and calf thymus DNA was studied by UV-vis and fluorescence spectroscopy. The results show that the interaction between complex **I** or **II** and calf thymus DNA is caused by insertion and binding.

REFERENCES

(1) Dasari, S.; Bernard, T. P. Cisplatin in cancer therapy: molecular mechanisms of action. *Eur. J. Pharmacol.* **2014**, 740, 364–378.

(2) van den Berg, J. H.; Beijnen, J. H.; Balm, A. J. M.; Schellens, J. H. M. Future opportunities in preventing cisplatin induced ototoxicity. *Cancer Treat. Rev.* **2006**, 32, 390–397.

(3) Shahid, F.; Farooqui, Z.; Khan, F. Cisplatin-induced gastrointestinal toxicity: an update on possible mechanisms and on available gastroprotective strategies. *Eur. J. Pharmacol.* **2018**, 827, 49–57.

(4) Rajeswaran, A.; Trojan, A.; Burnand, B.; Giannelli, M. Efficacy and side effects of cisplatin- and carboplatin-based doublet chemotherapeutic regimens versus non-platinum-based doublet chemotherapeutic regimens as first line treatment of metastatic non-small cell lung carcinoma: a systematic review of randomized controlled trials. *Lung Cancer-J. Iaslc* **2008**, 59, 1–11.

(5) Milosavljevic, N.; Duranton, C.; Djerbi, N.; Puech, P. H.; Gounon, P.; Lagadic-Gossmann, D.; Dimanche-Boitrel, M. T.; Rauch, C.; Tauc, M.; Counillon, L.; Poët, M. Nongenomic effects of cisplatin: acute inhibition of mechanosensitive transporters and channels without actin remodeling. *Cancer Res.* **2010**, 70, 7514–7522.

(6) Levi, J. A.; Aroney, R. S.; Dalley, D. N. Haemolytic anaemia after cisplatin treatment. *Br. Med. J.* **1981**, 282, 2003–2004.

(7) Karasawa, T.; Steyger, P. S. An integrated view of cisplatin-induced nephrotoxicity and ototoxicity. *Toxicol. Lett.* **2015**, 237, 219–227.

(8) Banti, C. N.; Hadjikakou, S. K.; Sismanoglu, T.; Hadjiliadis, N. Anti-proliferative and antitumor activity of organotin(IV) compounds. An overview of the last decade and future perspectives. *J. Inorg. Biochem.* **2019**, 194, 114–152.

(9) Jiang, W. J.; Mo, T. Z.; Zhang, F. X.; Kuang, D. Z.; Tan, Y. X. Syntheses, crystal structures and in vitro anticancer activities of dibenzyltin compounds based on the N-(2-phenylacetic acid)-aroyl hydrazone. *Chin. J. Struct. Chem.* **2020**, 39, 673–681.

(10) Jiang, W.; Fan, S.; Zhou, Q.; Zhang, F.; Kuang, D.; Tan, Y. Diversity of complexes based on *p*-nitrobenzoylhydrazide, benzoylformic acid and diorganotin halides or oxides self-assemble: cytotoxicity, the induction of apoptosis in cancer cells and DNA-binding properties. *Bioorg. Chem.* **2020**,

94, 103402.

(11) Li, Y. X.; Yu, H. T.; Zeng, H. T.; Liu, M. Q.; Kuang, D. Z.; Tan, Y. X.; Jiang, W. J. Two new dibenzyltin complexes based on the 2-oxo-3-phenylpropionic acid arylformylhydrazone: syntheses, crystal structures and biological activity. *Chin. J. Struct. Chem.* **2019**, 38, 1947−1955.

(12) Jiang, W. J.; Tan, Y. X.; Yu, J. X.; Zhu, X. M.; Zhang, F. X.; Kuang, D. Z. Syntheses, crystal structures and biological activity of 2-oxo-3-phenylpropionic acid aroyl hydrazone di-2,4-dichlorobenzyltin complexes. *Chin. J. Inorg. Chem*. **2016**, 32, 1383−1390.

(13) Sheldrick, G. M. *SHELXL-97, A Program for Crystal Structure Refinement*. Germany Ge öttingen: University of Ge öttingen **1997**.

(14) Pyle, A. M.; Rehmann, J. P.; Meshoyrer, R.; Kumar, C. V.; Turro, N. J.; Barton, J. K. Mixed-ligand complexes of ruthenium(II): factors governing binding to DNA. *J. Am. Chem. Soc.* **1989**, 111, 3051−3058.

(15) Wu, Q.; Yin, H.; Yue, C.; Zhang, X.; Hong, M.; Cui, J. Synthesis, crystal structure, and bioactivity of two triphenylantimony derivatives with benzohydroxamic acid and N-phenylbenzohydroxamic acid. *J. Coord. Chem.* **2012**, 65, 2098−2109.

(16) Yin, H.; Liu, H.; Hong, M. Synthesis, structural characterization and DNA-binding properties of organotin(IV) complexes based on Schiff base ligands derived from 2-hydroxy-1-naphthaldy and 3- or 4-aminobenzoic acid. *J. Organomet. Chem.* **2012**, 713, 11−19.

(17) Yan, C.; Zhang, J.; Liang, T.; Li, Q. Diorganotin(IV) complexes with 4-nitro-N-phthaloyl-glycine: synthesis, characterization, antitumor activity and DNA-binding studies. *Biomed. Pharmacother.* **2015**, 71, 119−127.

(18) Tan, Y. X.; Zhang, Z. J.; Feng, Y. L.; Yu, J. X.; Zhu, X. M.; Zhang, F. X.; Kuang, D. Z.; Jiang, W. J. Syntheses, crystal structures and biological activity of the 1*D* chain benzyltin complexes based on 2-oxo-propionic acid benzoyl hydrazone. *J. Inorg. Organomet. P* **2017**, 27, 342−352.

(19) Tan, Y. X.; Zhang, Z. J.; Liu, Y.; Yu, J. X.; Zhu, X. M.; Kuang, D. Z.; Jiang, W. J. Synthesis, crystal structure and biological activity of the Schiff base organotin(IV) complexes based on salicylaldehyde-*o*-aminophenol. *J. Mol. Struct.* **2017**, 1149, 874−881.

(20) Pretsch, E.; Bühlmann, P.; Badertscher, M. *Structure Determination of Organic Compounds*. Fourth ed. Berlin Heidelberg: Springer-Verlag **2009**, p69−242.

(21) Basu Baul, T. S.; Addepalli, M. R.; Lyčka, A.; van Terwingen, S.; Englert, U. Synthesis, characterization and structural systematics in diorganotin complexes with O,N,O′-tris-chelating semirigid diaza-scaffolds: mono- *vs*. di-nuclear compounds. *J. Organomet. Chem.* **2020**, 927, 121522−11.

(22) Zhang, Z. J.; Zeng, H. T.; Liu, Y.; Kuang, D. Z.; Zhang, F. X.; Tan, Y. X.; Jiang, W. J. Synthesis, crystal structure and anticancer activity of the dibutyltin(IV) oxide complexes containing substituted salicylaldehyde-*o*-aminophenol Schiff base with appended donor functionality. *Inorg. Nano-Met. Chem*. **2018**, 48, 486−494.

(23) Jiang, W. J.; Zhou, Q.; Liu, M. Q.; Zhang, F. X.; Kuang, D. Z.; Tan, Y. X. Microwave assisted synthesis of disubstituted benzyltin arylformylhydrazone complexes: anticancer activity and DNA-binding properties. *Appl. Organomet. Chem.* **2019**, 33, e5092.